Engineering Structures 80 (2014) 486–500

Contents lists available at ScienceDirect

Engineering Structures

journal homepage: www.elsevier.com/locate/engstruct

Seismic performance-based assessment of "Gaioleiro" buildings

Ana Simões [a,*], Rita Bento [a], Serena Cattari [b], Sergio Lagomarsino [b]

[a] Instituto de Engenharia de Estruturas, Território e Construção (ICIST), Instituto Superior Técnico, Universidade de Lisboa, Portugal
[b] Department of Civil, Chemical and Environmental Engineering (DICCA), University of Genoa, Italy

ARTICLE INFO

Article history:
Received 30 December 2013
Revised 13 September 2014
Accepted 15 September 2014

Keywords:
Masonry buildings
"Gaioleiro" buildings
Seismic performance-based assessment
Non-linear static analysis
Limit non-linear kinematic analysis

ABSTRACT

"Gaioleiro" buildings are unreinforced masonry buildings with flexible timber floors associated with the urban expansion of Lisbon at the end of the nineteenth century and beginning of the twentieth century. This paper presents the results from the seismic performance-based assessment of a "Gaioleiro" building case study, assumed as a prototype representative of wide number of buildings. The assessment was addressed to the global seismic response of the building, mainly governed by the in-plane capacity of the masonry walls, and to the local response, related to the activation of out-of-plane mechanisms of parts of the building. The global behaviour was determined by non-linear static analyses and the effects of some relevant modelling options were considered; in particular, parametric analyses were carried out taking into account the strength capacity of spandrel beams and the influence of the degree of connection between walls. The local behaviour was determined with limit non-linear kinematic analysis. The seismic performance-based assessment was set by the comparison of the structural capacity, with reference to various limit states (as proposed in Eurocode 8), with the seismic demand for Lisbon, related to different return periods. Different approaches to define such limits on the capacity curve were assumed in order to discuss the reliability of criteria proposed in codes for the case of structures characterized by flexible floors.

1. Introduction

Old masonry buildings were built for many centuries based on available materials and empirical provisions justifying the strong uncertainties about their structural behaviour. It is estimated that half of the existing stock in Lisbon is composed of unreinforced masonry buildings built before the introduction of proper seismic code provisions. The structural assessment of these buildings is a crucial issue in areas with a moderate to high seismic hazard like Lisbon. The work herein presented is addressed to the seismic performance-based assessment of "Gaioleiro" buildings: mid to high-rise unreinforced masonry buildings with flexible timber floors and roof. These buildings are assembled in aggregated blocks where four types of building structures can be identified [1]. In this paper, the assessment of one type of "Gaioleiro" buildings was carried out considering both the global response and the possible occurrence of local out-of-plane mechanisms, by neglecting their interaction. In fact, as is common practice, since out-of-plane mechanisms usually involve local parts of the structure, they are verified separately referring only to that specific portion. Even if local mechanisms typically occur first, in this paper their assessment is presented after the global analysis, as it is necessary to get from the latter the amplification of the seismic demand at the level where the mechanisms occur.

To assess the global response, the building was modelled according to the equivalent frame approach in Tremuri Program [2]. Assuming the seismic inertial loads are transferred to walls through the horizontal diaphragms, the behaviour is governed by the in-plane capacity of the walls discretized in panels: piers and spandrels, where the non-linear response is concentrated, and rigid nodes defining the connections. The timber floors were modelled as membrane elements with quite flexible behaviour. The building capacity curves were obtained by performing non-linear static (pushover) analyses in both main directions. Parametric analyses were carried out taking into account the strength capacity of spandrel beams and the type of connection between perpendicular walls (flange effect) aiming to verify the influence of these modelling issues on the behaviour of the building [3,4]. The local response of the façade wall was analysed by adopting a macro-block approach in MB-Perpetuate Program [5]. The wall out-of-plane capacity curves were determined through limit non-linear kinematic analysis after considering a set of possible collapse mechanisms, before and after the introduction of some strengthening solutions to prevent the out-of-plane failure.

* Corresponding author. Tel.: +351 917 597 113.
E-mail address: ana.g.simoes@ist.utl.pt (A. Simões).

http://dx.doi.org/10.1016/j.engstruct.2014.09.025
0141-0296/

The seismic performance-based assessment was obtained by comparing the capacity of the building, defined by the in-plane and out-of-plane capacity curves, with the seismic demand for Lisbon in order to check the fulfilment of performance limit states. These limits were set based on the criteria recommended by the Eurocode 8 [6,7] and on the multiscale approach proposed by the Perpetuate Project [8]. This multiscale approach correlates the damage on the building at different scales: single elements (piers and spandrels), macroelements (walls and diaphragms) and global. This procedure is particularly effective in case of structures with flexible floors, as the "Gaioleiro" buildings, in comparison with common criteria proposed in codes.

2. The "Gaioleiro" buildings

"Gaioleiro" buildings are characteristic of the construction in Lisbon at the end of the nineteenth century and the beginning of the twentieth century. The economic development of the country and the urban expansion plan developed by the engineer Ressano Garcia originated new aggregates of terraced buildings [1]. These buildings are mainly located in the neighbourhood of "Avenidas Novas" connecting the "Pombalino" downtown area, close to the Tagus River, to the north upland area of the city. The "Gaioleiro" buildings define a transitory period from the anti-seismic practises used on "Pombalino" buildings, built after the 1755 earthquake [9], and the modern reinforced concrete buildings. It is estimated there are about fourteen thousand "Gaioleiro" buildings in Lisbon, representing 24% of the existing building stock of Lisbon [10].

The "Gaioleiro" buildings are mid to high-rise masonry structures, with four to six floors and different interstorey height. The exterior walls are made of rubble stone masonry and air lime mortar with variable thickness up the height [11]. There are also buildings in which the side walls are made of clay brick masonry. The interior walls are made of clay brick masonry: solid bricks on ground floors and hollow bricks on top floors. The partition walls have a light timber structure made of vertical and diagonal boards and crossed laths. Floors are made of timber beams perpendicular to the façade walls. The roof is made of king timber trusses also perpendicular to the façade walls and covered in ceramic tiles.

These buildings have elongated rectangular plan shapes with shafts on the side or inside the building to provide ventilation and natural light to interior rooms. "Gaioleiro" buildings can be divided in four types depending on the plan configuration of the structure [1]: type I – buildings with small size façade walls and one side shaft, type II – buildings with medium size façade walls and one shaft, type III – buildings with large façade walls and more than one shaft and type IV – buildings on the corner of the aggregate. Figs. 1 and 2 present typical façade and plan geometry of these buildings. Fig. 3 shows an example of the steel balconies commonly used on the back façade wall. These balconies are made of I steel profiles connected with arches of clay bricks, which were supported on the façade wall and on a steel frame.

The fast development of the city followed by a period of real estate speculation ended up affecting the seismic safety of these buildings regarding the materials and constructive details used. Thus, "Gaioleiro" buildings are nowadays classified as the typology with highest structural weaknesses from the building stock of Lisbon. Motivated by the uncertainties on the seismic behaviour of these buildings, several research works have been carried out. Candeias [12] performed a set of shaking table tests on reduced scale buildings analysing different strengthening solutions to prevent the out-of-plane collapse of façade walls. Mendes and Lourenço [13] developed a numerical study based on these experimental results including non-linear step-by-step dynamic analyses and several types of pushover analyses. Mendes et al. [14] also performed shaking table tests on a reduced scale "Gaioleiro" building; after the first series of seismic tests, the building was repaired

Fig. 1. Typical front façade wall of "Gaioleiro" buildings type I, II, III and IV.

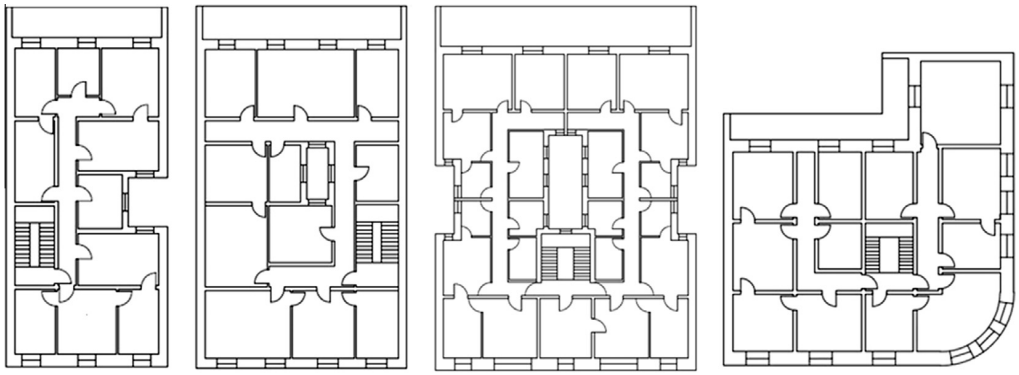

Fig. 2. Typical plan geometry of "Gaioleiro" buildings type I, II, III and IV.

Fig. 3. Steel balcony on the back façade wall.

(aiming to re-establish the initial conditions), strengthened and tested again. A numerical model was defined and calibrated based on the test results and used to compare different types of non-linear analyses. Branco and Guerreiro [15] developed a numerical study to verify the effect of different strengthening solutions on the seismic behaviour of a "Gaioleiro" building, namely: introduction of reinforced concrete walls on the shafts, base isolation and some techniques to strength timber floors.

The above-mentioned works highlighted the seismic vulnerability of "Gaioleiro" buildings and the importance of using suitable numerical models. The work herein presented addresses the seismic assessment of "Gaioleiro" buildings of type I, as presented in Fig. 4. The building case study was analysed as an isolated structure to verify the influence of some modelling issues related to the structural behaviour. Even if these buildings are included in aggregate blocks, results can be considered of interest because of the relative uniformity of buildings and, anyway, due to the existing voids in the blocks, some buildings are not confined on one side.

The building has an asymmetric and elongated rectangular plan shape (Fig. 4): two façade walls with about 30% of opening area, one side wall with no openings and one side wall cut by a shaft. Thus, it is to expect a quite different behaviour in the two structural directions. The building has five floors with different interstorey height: ground floor is 3.6 m, 1st floor is 3.5 m and 2nd, 3rd and 4th floors' are 3.3 m, with a total height of 17 m. The exterior walls are made of rubble stone masonry and air lime mortar. The thickness of the front façade wall (P2 in Fig. 4(c) where all the walls are numbered) is 0.8 m on the ground floor, decreasing 0.1 m in each floor till a minimum of 0.5 m. The thickness of the back façade wall (P5) is 0.6 m on the ground and 1st floors, decreasing to 0.5 m on the 2nd floor. Under the window openings, the thickness of the walls is reduced to 0.3 m. The side walls (P3 and P4) have a constant thickness of 0.5 m.

The interior walls are made of clay brick masonry also with variable thickness which depends on the arrangement adopted for the bricks (brick size: $0.23 \times 0.11 \times 0.07$ m). The plan distribution of interior walls is shown in Fig. 4(c). The main walls – P6, P7, P8, P9, P10, P12, P14 – have a constant thickness of 0.23 m, reduced on the last floor to 0.11 m, and are made of solid bricks on the ground and 1st floors and hollow bricks on the others. The secondary walls – P13, P15, P16 – have a constant thickness of 0.11 m, reduced on the last floor to 0.07 m, and are made of hollow bricks. The walls from the shaft and from the sides of the back balconies are made of solid brick masonry with a thickness of 0.35 m, reduced on the last floor to 0.23 m.

The number of experimental tests on "Gaioleiro" buildings is very limited. Silva and Soares [16] estimated for rubble stone masonry walls a compressive strength (f_m) between 0.8 MPa and 1.5 MPa and Young modulus (E) between 0.7 GPa and 1 GPa. Lopes and Azevedo [17] carried out monotonic tests on the exterior wall from a "Gaioleiro" building obtaining a Young modulus equal to 0.6 GPa. Other experimental studies are related to test of reduced scale models of "Gaioleiro" buildings for shaking table tests [12,14]. Due to this, the masonry parameters were defined based on some values proposed in literature for similar masonry types, by adopting in particular those recommended in the Italian code [18] for rubble stone masonry, solid and hollow clay brick masonry and calibrated by the referred experimental results. Table 1 summarizes the mechanical properties of the masonry considered in this study. The values for the stiffness properties (E and G) are representative of a cracked condition after applying a reduction factor to elastic values. In case of rubble stone masonry, the factor is equal to 0.5, basis on the proposed in [6]. In case of clay brick masonry, the factor is equal to 0.75 justified by the results of previous parametric analyses [2] and the prevalence of a flexural

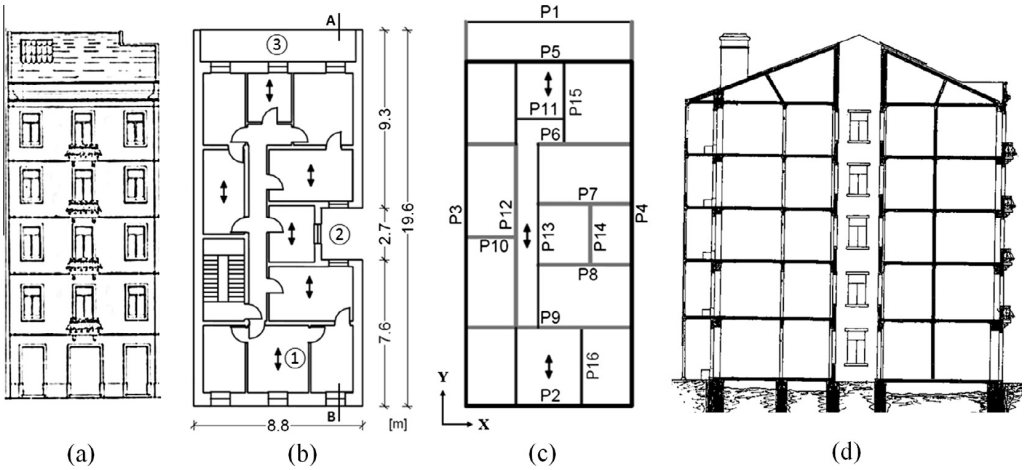

Fig. 4. "Gaioleiro" building type I: (a) front view, (b) plan view, (c) identification of the walls and (d) cut section view AB. Legend: 1 – orientation of floors, 2 – side shaft, 3 – back balcony.

Table 1
Masonry mechanical properties and gravity loads adopted.

Mechanical parameters	Young modulus, E (GPa)	Shear modulus, G (GPa)	Compressive strength, f_m (MPa)	Shear strength, τ_0[a] (MPa)	Specific weight, γ (kN/m^3)	Gravity loads permanent/live (kN/m^2)
Rubble stone masonry	0.90	0.29	1.3	0.026	19.0	Floors: 0.7/2.0 Staircase: 0.7/4.0 Roof: 1.4/2.0 Balcony: 2.0/2.5
Solid clay brick masonry	1.13	0.38	3.2	0.076	18.0	
Hollow clay brick masonry	0.90	0.30	2.4	0.060	12.0	

[a] Diagonal cracking failure mode according to the criterion proposed in [19] and adopted in [18].

response of masonry panels (§3.1) that tend to concentrate cracks in end sections.

Floors are made of timber beams with 0.18 m height and 0.07 m width, placed perpendicular to the façade walls with an average offset of 0.4 m. These beams are restrained in the perpendicular direction by smaller beams and covered by timber boards with 0.02 m thickness. The timber elements were considered with Young modulus of 8 GPa. The balconies on the back façade wall (Fig. 3) have a composite structure made of steel beams (IPE180, S235) with 0.4 m offset, connected by arches of clay brick and cement topping with 0.05 m thickness and 25 GPa Young modulus. These balconies are supported on one side by the façade wall and on the other by steel beams, supported at mid span by steel circular columns with exterior diameter of 0.09 m and thickness of 0.01 m. Table 1 also presents the gravity loads, both permanent and live, adopted in the numerical model.

3. Global seismic behaviour

The global seismic response of the building, mainly governed by the in-plane capacity of walls, takes place when the connection between walls and load transfer through floors and roof diaphragms are effective [20]. The behaviour of the "Gaioleiro" building was assessed by performing non-linear static (pushover) analysis through Tremuri Program: commercial version [21] to generate the model and research version to perform the non-linear analyses [22] by using proper advanced constitutive laws for masonry elements [23]. The solutions adopted in the program are discussed in detail in [2].

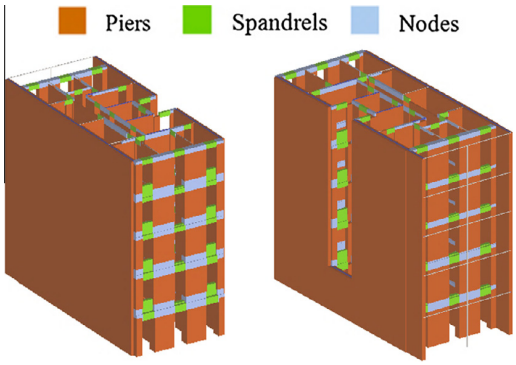

Fig. 5. Three-dimensional front and back view of the building.

The three-dimensional model of the building was obtained by assembling: (1) the masonry walls idealized as equivalent frames and (2) the horizontal diaphragms modelled as membrane elements. To define the masonry walls it is first necessary to identify: piers, which are the vertical resisting elements carrying both vertical and lateral loads; spandrels, which are the horizontal elements, coupling piers and limiting their end-rotations in case of lateral loads; and the rigid nodes, undamaged masonry portions confined among piers and spandrels. The geometry is defined by the distribution of openings and on conventional criteria supported by observation of unreinforced masonry buildings damaged after earthquakes and after experimental tests on masonry panels. Fig. 5 shows the equivalent frame model of the building.

The response of the panels was modelled by non-linear beams with multilinear constitutive law, a recent formulation implemented in Tremuri Program [23]. Fig. 6 illustrates the force–deformation relationships assumed: it is based on a phenomenological approach that aims to describe the non-linear response of masonry panels until very severe damage levels (DLs from 1 to 5: DL1 – slight, DL2 – moderate, DL3 – extensive, DL4 – near collapse and DL5 – collapse).

Each DL is defined in terms of drift limits (δ_E) and corresponding strength decay (β_E); these values are distinguished for each panel depending on the occurred failure mode. Once DL5 is reached, the element only keeps its capacity to support vertical loads. The initial elastic branch is directly defined by the flexural and shear stiffness of the panels. The ultimate shear (V_u) is computed after some simplified criteria proposed in codes and literature and mechanical or phenomenological hypotheses by considering the occurrence of flexural or shear failure modes or the occurrence of mixed modes, when the prediction between the two is quite close. The drift limits are, in this last case, evaluated as a linear combination of those associated with the basic failure modes. The limits for drift (δ_E) and strength decay (β_E) associated with each DL are illustrated in Fig. 6 and were defined based on reference values proposed in codes [18,24] and experimental campaigns [29].

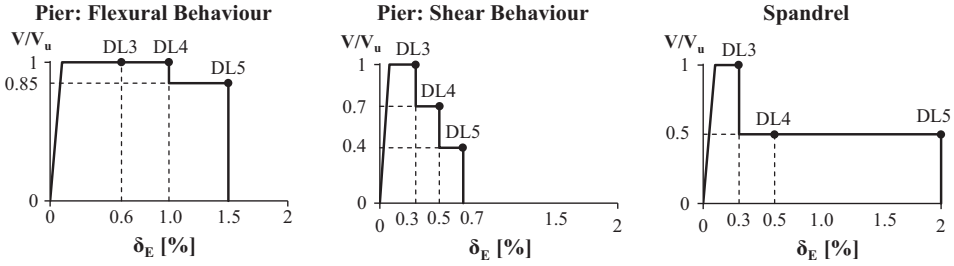

Fig. 6. Force–deformation multilinear constitutive laws for piers and spandrels.

The shear behaviour is assumed to be governed by diagonal cracking failure according to Turnšek and Sheppard criterion [19], recommended in [18] for existing masonry buildings. In case of flexural behaviour, different laws have been considered in case of piers and spandrels. For piers, following the common criteria proposed in codes [7,18,24], the ultimate bending moment at the panel end section is calculated by neglecting the tensile strength of masonry and assuming a stress-block distribution at the compressed toe (considering the compressive strength of masonry normal to bed joints). For spandrels, a sensitivity analysis was carried considering the elements modelled with no tensile strength (Model A), analogously to what is assumed for piers, and considering an equivalent tensile strength (Model B), according to the criterion proposed by Cattari and Lagomarsino [25]. Such assumption is motivated by the interlocking of masonry blocks at the panel end sections (more in case of brick masonry). Indeed, in last decades, several tests have been performed to characterize the response of spandrels [26–28] and, in particular, the reliability of the criterion proposed in [25] was demonstrated by experimental tests presented in [27]. The results have also shown greater deformation capacity of these elements in comparison with piers. In case Model B, the referred criterion was assigned to both typologies of masonry walls: in case of exterior rubble stone masonry walls, due to its irregular pattern, the parameter that defines the interlocking was assumed to be half of the one assigned for interior brick masonry walls directly from the brick size.

The connection between perpendicular walls also poses several uncertainties on the behaviour of the building [20], especially when walls are made of different masonry types. The effectiveness of the interlocking is questionable as the interior brick walls were, probably, built after the rubble stone masonry walls. Thus, to assess the influence of this interface, the link between interior and exterior walls was defined by equivalent beams at the floor level: walls P6, P9 and P10, in the X direction, and P12, P15 and P16, in the Y direction (Fig. 7). The properties of these equivalent beams (area and moment of inertia) were accounted for two limit conditions: (1) good connections between walls (Model A and B), by assuming values equivalent to a rigid link, and (2) weak connections (Model C), by adopting low values for the area and moment of inertia.

Floors are modelled as equivalent orthotropic membranes, of assumed reference thickness, characterized by: (1) normal stiffness, defined by Young modulus $E_{1,eq}$ in the main warping direction and $E_{2,eq}$ in the perpendicular direction and (2) in-plane shear stiffness, related to shear modulus $G_{12,eq}$. The normal stiffness is associated with the degree of wall-to-floor connection and provides a link between nodes of the same wall, thus influencing the axial force on spandrels. The latter determines the distribution of horizontal forces among walls due to their relative position, stiffness and strength. The timber floors were defined by a membrane with 0.02 m thickness and characterized by $E_{1,eq}$ = 20.6 GPa; $E_{2,eq}$ = 80.6 GPa, and $G_{12,eq}$ = 0.04 GPa. The shear stiffness was assigned based on the recommendations of [30] for single straight sheeting. After performing a sensitivity analysis by varying $G_{12,eq}$ with c.o.v. equal to 0.5, it was concluded that the overall behaviour of the building was almost unchanged. The balconies on the back façade were defined with 0.04 m thickness and by $E_{1,eq}$ = 30.8 GPa and $G_{12,eq}$ = 13.4 GPa (as suggested by Tremuri commercial version after the geometric and mechanical properties of the floor). The acting loads were distributed only in the warping direction of the floors.

In summary, the following modelling options were considered in the next section:

- Model A: spandrels modelled by the criterion proposed in [7,18] and good connections between walls.
- Model B: spandrels modelled by the criterion proposed in [25] and good connections between walls.
- Model C: spandrels modelled by the criterion proposed in [25] and weak connections between walls.

3.1. Non-linear static (Pushover) analysis

The non-linear static (pushover) analysis consists in applying to the building a static distribution of lateral loads, representative of the inertial seismic actions, by increasing their magnitude till the maximum strength of the building, and then increasing displacements by keeping the same load pattern, in order to evaluated the progressive strength degradation and the ultimate displacement capacity. The response of the structure is derived from the pushover curve (total base shear vs. horizontal displacement of a control node), which provides information about the capacity of the building in terms of stiffness, overall strength and ultimate displacement capacity. The analyses were performed with two load distributions: (1) uniform – pattern of forces applied to each node of the building and proportional to its mass and (2) pseudo-triangular – pattern of forces proportional to the product between the mass of the node and its height with respect to the base.

The option for the pseudo-triangular load, instead of a distribution strictly proportional to the first modal shape, as recommended by codes [6,7], is, in this case, justified by the low participant mass involved in the first modes of the building (Fig. 8). This is consequence of the quite flexible behaviour of the timber floors, which are not able to couple the dynamic behaviour of the different walls. Due to this fact, only some of the walls would be involved on the pushover analysis, while with the pseudo-triangular load pattern all masses are considered on the response of the building. As an alternative, a multimodal approach (e.g. Reyes and Chopra [31]) or a load pattern obtained by combining more modes (e.g. through the SRSS rule) could be adopted. Fig. 8 depicts the modal deformed shape of the building (in the case of Model A) showing the first modes associated with the translation of the building: (a) X direction with fundamental period equal to 0.69 s and mass participation of 54% and (b) Y direction with fundamental period equal to

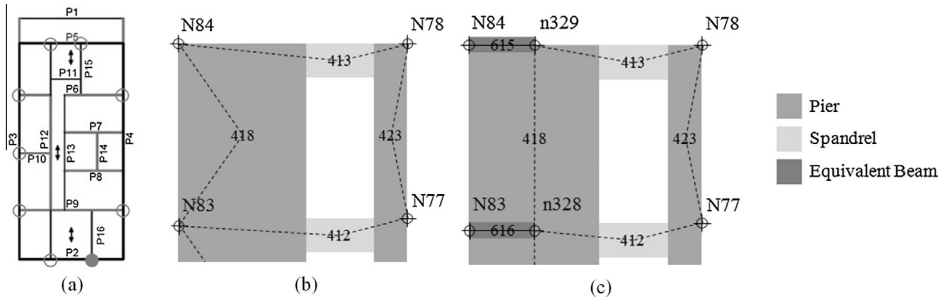

Fig. 7. Connection between walls: (a) identification of the walls and example of wall P16 on the 4th floor, (b) original model and (c) equivalent beams at the floor level.

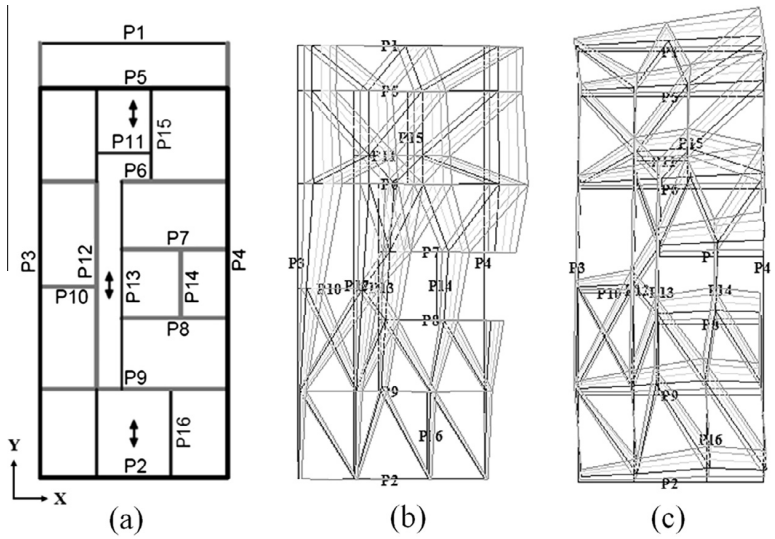

Fig. 8. Modal shape: (a) plan undeformed shape, (b) 1st mode with translation in *X* direction and (c) 1st mode with translation in *Y* direction.

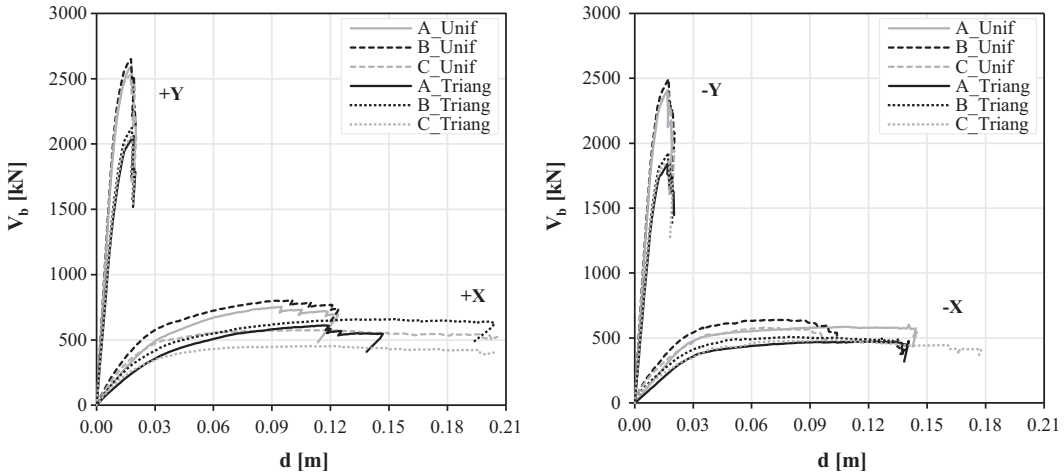

Fig. 9. Pushover curves for Model A, B and C.

0.33 s and mass participation of 64%. The results of modal analysis are almost insensitive to the three different modelling assumptions.

Fig. 9 shows the "Gaioleiro" building pushover curves for Model A, B and C in *X* and *Y* directions (both positive (+) and negative (−)). The curves plot the average displacement of all nodes located at the roof level (d) against the base shear (V_b). This choice aims to obtain, in case of buildings with flexible floors, a curve more representative of the behaviour of the whole structure and not only of a single wall. The pushover analyses were stopped for 20% decay of the maximum base shear, in agreement with [7,18] which define this condition as that associated with the ultimate displacement capacity of the structure (as discussed more in detail in §3.2).

It is evident from Fig. 9 that the building has higher stiffness and strength in the *Y* direction than in the *X* direction. With reference to Model A, the variation is, approximately, equal to 93% in terms of stiffness and 73% in terms of strength. These differences are in part related to: (1) the rectangular configuration of the building, (2) the presence of blind walls in the *Y* direction in contrast with (3) the higher number of openings in the *X* direction. The pushover curves in the positive and negative directions also show several variations, in particular in the *X* direction due to the asymmetry of the structure. This puts in evidence the importance of analysing the building in all directions and to consider the worst scenario. Some curves in Fig. 9 show the "snap back" phenomenon, i.e. the average displacement on the last floor of the building decreases together with the reduction of the base shear. To explain this it is important to recall that, even if in the pushover curves the average displacement is plotted, the execution of pushover analysis requires choosing a single control node. In this case the control node in the wall that fails was chosen in order to improve the convergence: so while the displacement of the control node has a little increase, the displacements on the nodes from other walls decrease.

The results with both load distributions describe an envelope of the expected behaviour of the building: the higher limit is defined by the uniform load distribution and the lower by the pseudo-triangular load (Fig. 9) with a 38% variation of stiffness and 27% of strength. As to the ductility, the difference is more evident in the *X* direction, with an average variation of 18%. Fig. 10 plots the contribution of all walls to the total base shear ($V_{bi}/V_{b,total}$) in Model A for the pseudo-triangular load distribution in the positive *X* and *Y*

directions, showing a more significant redistribution of forces among walls in the *X* direction. The damage pattern for the last step of the pushover analysis with the pseudo-triangular load distribution is depicted in Figs 11 and 12 for the main walls of the building. The legend displays the type of failure and the damage level. It is worth noting that the ultimate displacement varies with the load pattern considered.

The side walls P3 and P4 have the main participation in the *Y* direction (Fig. 10). Due to this, the response of the structure is, practically, invariant to the modelling solution considered (Model A, B and C). With the position of the shaft on the side of the building, the structure is subjected to torsional effects inducing higher displacements on wall P4 and the shear failure of the wall at the end of the analysis ($4 < DL < 5$), as shown in Fig. 11. Damage on the remaining walls is between $2 < DL < 3$.

In the *X* direction, the contribution to the total base shear is extended to all walls (Fig. 10). Damage pattern is characterized by flexural failure of spandrel beams (at the beginning of the non-linear behaviour), and by flexural and mixed shear-flexural damage of piers (Fig. 12). This type of behaviour derives from the presence of slender piers and from the very moderate coupling provided by spandrels (which show a "weak" behaviour due to the lack of other tensile resistant elements coupled to them). In this example, the ratio ($V_{bi}/V_{b,total}$) is higher on the interior wall P9 than on the adjacent façade wall P2 (Fig. 10) and, in the end, the collapse of the building in the *X* direction is triggered by the mixed shear-flexural failure of piers of wall P9 at the 1st floor (Fig. 12). The concentration of damage at this level is justified by the structural irregularity of the building motivated by the different uses: shops/ware house on the ground floor and residential use on the other floors.

In what concerns the modelling solutions, several effects are noticed in the *X* direction. From Model A to B, the initial stiffness increases approximately 20%, in consequence of the "equivalent" tensile resistance attributed to spandrels. This provides a better coupling to piers in the beginning of the analysis, yet the damage pattern suffers few variations. Model C, with weak connections between interior and exterior walls (spandrels are defined as in

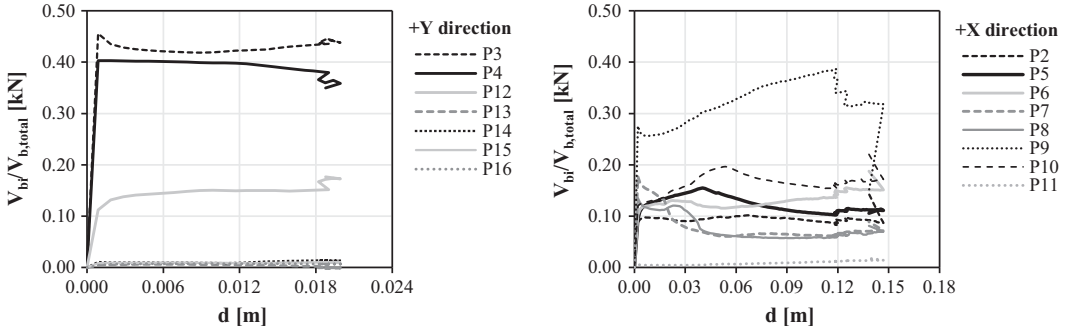

Fig. 10. Contribution of the walls to the total base shear in Model A (walls P2–P16 are identified in Fig. 8).

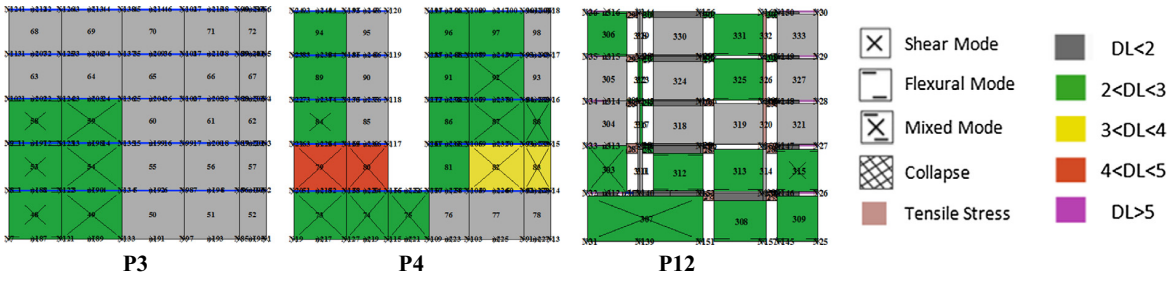

Fig. 11. Damage pattern for the ultimate displacement in Model A: +*Y* direction.

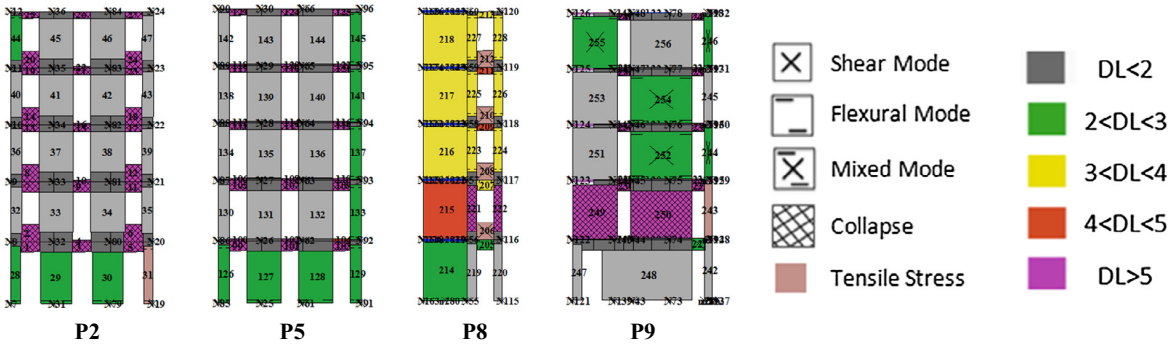

Fig. 12. Damage pattern for the ultimate displacement in Model A: +*X* direction.

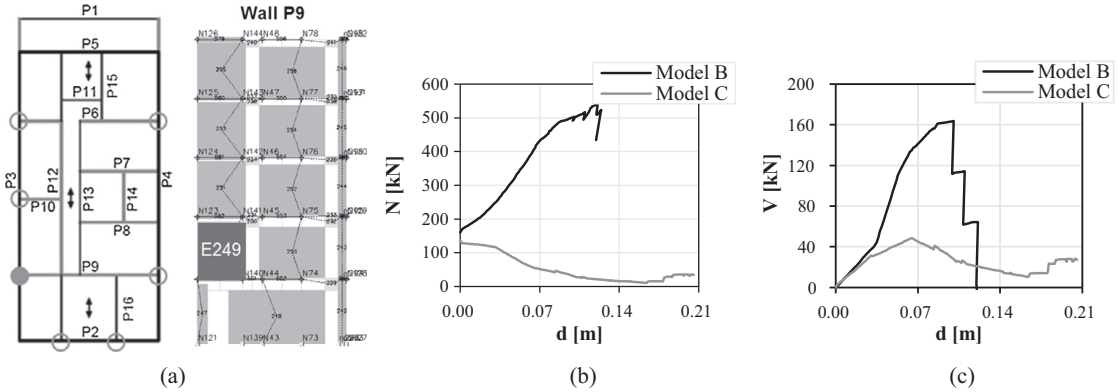

Fig. 13. Internal forces on (a) pier E249 (wall P9) for the +*X* uniform analysis, (b) axial force N and (c) shear force V.

Model B), leads to higher ductility and to a spread of damage on the structure. The most evident difference from Model B to C is the reduction of the initial stiffness and strength. This can be explained by the reduction of the flange effect induced by the exterior walls on the perpendicular walls. As a consequence, forces on piers from the interior walls decrease, as exemplified in Fig. 13 for pier E249 from wall P9, which defines the connection with the side wall P3 at the 1st floor.

Based on the above-mentioned, it is possible to conclude that the behaviour of the building in the *Y* direction is almost indifferent to the modelling solutions as the response is mainly governed by the side walls. In the *X* direction, the results from Model B and C define an upper and lower limit of the response. It can be inferred that the expected in-plane capacity of the building may be well derived from Model B and Model C, rather than Model A. Therefore, only these results will be considered on the following section.

3.2. Seismic performance-based assessment

The seismic performance-based assessment consists in determining the performance point, from the intersection of the structure capacity curve with the seismic demand, and the verification for the fulfilment of performance levels (or limit states) associated with increasing expected hazard levels. The definition of limit states in buildings with box-type behaviour and rigid floors is quite trivial, as it is reasonable to assume that a number of elements and walls reach a certain limit state almost at the same time. The Eurocode 8 [7] proposes three limit states in function of the level of damage in the structure: damage limitation (DL), significant damage (SD) and near collapse (NC). These limits are directly defined on the capacity curve basis on conventional displacement limits (heuristic approach) corresponding to: yielding displacement (d_y) for DL; ultimate displacement (d_u) defined for 20% decay of the maximum base shear in agreement with [7,18], for NC; and $3/4d_u$ for SD. In buildings with flexible floors, the limited load transfer leads to a more independent behaviour of the walls. Due to this, the reaching of serious damage in a wall may not appear evident on the capacity curve when this wall offers a small contribution to the total base shear. Therefore, the attainment of a certain limit state should also consider the lack of homogeneity on damage distribution and its possible premature concentration in some walls (as stated in §3.1). Thus, the adoption of the criteria proposed in [7] to define the limit states may induce, in case of buildings with flexible floors, to non-conservative results. To overcome this problem, in this work, the limit states were defined based on the criteria proposed by [7] and on a multiscale approach proposed on Perpetuate Project [8], by assuming the attainment of the lowest threshold.

The multiscale approach correlates the damage on the building at different levels: elements (piers and spandrels), macroelements (walls) and whole building (represented by the pushover curve). This approach aims to monitor the occurrence of significant damage in parts of the building, which may not necessarily correspond to significant strength decay of the overall base shear. In this paper, only the macroelement scale was considered along with three interstorey drift limit thresholds: 0.2% for DL, 0.5% for SD and 0.8% for NC. These limits, referred in literature [32,33], are in agreement with the recommendations from ASCE/SEI 41/06 [24]. Mouyiannou et al. [34] also suggested a criterion based on additional checks, yet within the ambit of non-linear dynamic analyses. Table 2 summarizes the limit states adopted at global and wall scales and Fig. 14 exemplifies the procedure to determine these limits on the capacity curve based on the attainment of the worst condition (lower displacement). The interstorey drift $\delta_{p,l}$ (being $p = 1, \ldots, Np$ the wall number and $l = 1, \ldots, Nl$ the floor level) was determined from the contribution of both horizontal displacement and rotation components. Indeed, the interstorey drift is usually computed only referring to the horizontal displacement, but this is only acceptable in case of a shear-type behaviour, when spandrels are strong elements.

Fig. 14 shows that in the *X* direction the thresholds are conditioned by the verifications at the wall scale. The differences between both criteria are particularly evident on NC limit state, as from global to wall scale, the structure ultimate displacement was reduced in 58%. In the *Y* direction, the thresholds are defined by the global scale criteria as the building interstorey drift is much lower in this direction due to the higher stiffness and strength of the structure. Similar conclusions may be derived for the other cases.

For the seismic assessment of the building, the pushover curves obtained in section §3.1 were converted to an equivalent single degree of freedom (SDOF) system following the N2 Method, originally proposed by Fajfar [35] and adopted in codes [6,18]. An elasto-perfectly plastic force–displacement relationship was assumed to define the SDOF bi-linear capacity curve: the initial stiffness was determined by the point corresponding to 70% of the maximum base shear reached on the first branch of the curve; the yield force was determined in such way the areas under the

Table 2
Criteria adopted to define the limit states on the capacity curve.

Limit state	Global	Wall
DL	d_y	$\delta_{p,l} = 0.2\%$
SD	$3/4d_u$	$\delta_{p,l} = 0.5\%$
NC	$d_u = d(0.8V_{b,max})$	$\delta_{p,l} = 0.8\%$

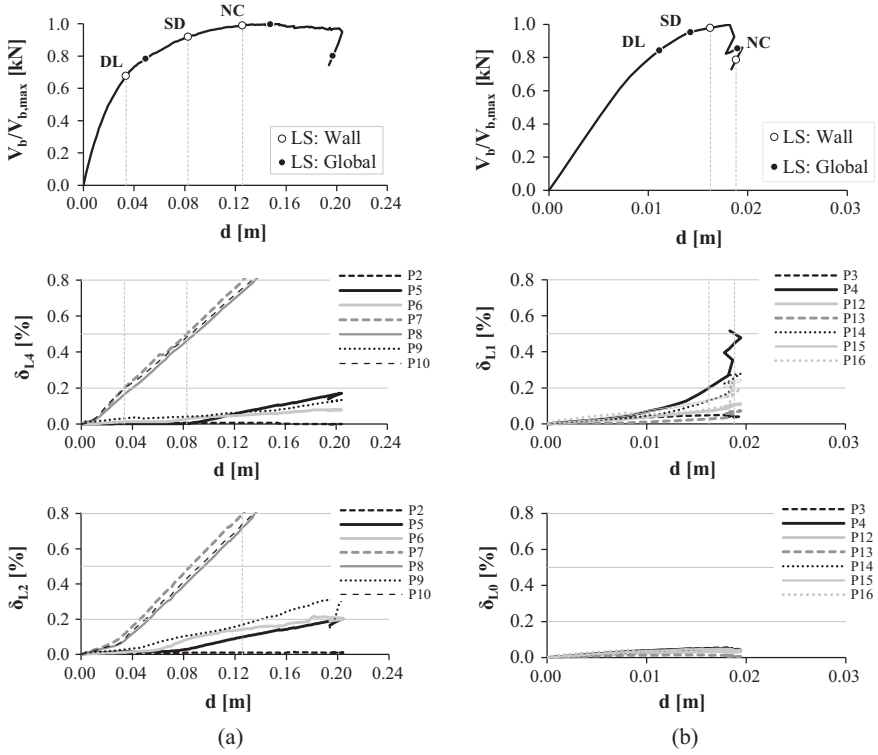

Fig. 14. Determination of the limit states in Model B for the pseudo-triangular load in (a) +*X* direction and (b) +*Y* direction.

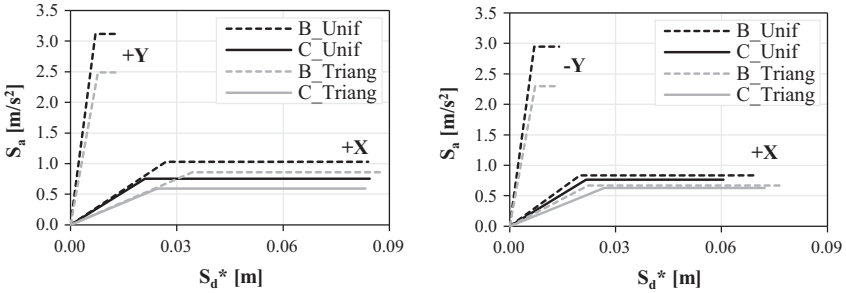

Fig. 15. SDOF capacity curves for Model B (spandrels modelled by the criterion proposed in [25] and good connections between walls) and Model C (spandrels modelled as in Model B and weak connections between walls).

pushover and the elasto-perfectly plastic curves are equal. Fig. 15 plots the SDOF capacity in the idealized elasto-perfectly plastic relation and Table 3 the corresponding properties, namely: equivalent period (T^*), ductility (μ^*) and strength computed from the ratio between yielding force and mass (F_y^*/m^*). Following the conclusions in the end of section §3.1, the results now presented are limited to Model B and C in the *X* direction, and to Model B in the *Y* direction. The building *X* direction presents higher equivalent period and ductility, which is in agreement with a more deformable structural system (lower plan dimension and higher number of openings). It is, therefore, reasonable to accept that in this direction the wall criterion prevails over the global one, as shown in Fig. 14. Strength is in general 71% higher in the *Y* than in the *X* direction.

The final step of the assessment consists of checking if the building withstands the seismic demand defined on the Eurocode 8 [6] for Lisbon. Both far-field (type 1.3) and near-field (type 2.3) seismic actions were considered with 5% equivalent viscous damping for soil type C. Each limit state was associated with an increasing expected hazard level (defined in terms of return period T_R): 225 years for DL, 475 years for SD and 2475 years for NC. Table 4 shows the reference ground accelerations for the two seismic actions and the three hazard levels on stiff soil (type A) and soil type C.

Fig. 16 exemplifies the performance point (d_{max}^*) obtained from the intersection of the bi-linear SDOF capacity curve for Model B with the seismic demand (type 1.3 with T_R = 475 years – SD limit state) in spectral coordinates (S_a – acceleration and S_d – displacement). The maximum displacements compatible with the fulfilment of SD limit state (d_{SD}) are also depicted showing the demand clearly exceeds the capacity of the structure ($d_{max}^* > d_{SD}$) in both directions: 1.7 times higher on the *X* direction and 2.5 times higher in the *Y* direction. Thus, it may be concluded that, for the seismic action type 1.3, the building (based on Model B) does not comply the performance level associated with SD limit state. In Fig. 16, q^* represents the ratio between the acceleration in the structure with unlimited elastic behaviour and with limited strength $S_e(T^*/F_y^*/m^*)$. The Italian code [18] recommends $q^* < 3$

Table 3
Properties of the SDOF capacity curves.

Load pattern and analysis direction		*X* direction						*Y* direction		
		Model B			Model C			Model B		
		T^* (s)	μ^*	F_y^*/m^* (m/s^2)	T^* (s)	μ^*	F_y^*/m^* (m/s^2)	T^* (s)	μ^*	F_y^*/m^* (m/s^2)
Uniform	+	1.02	3.12	1.03	1.05	4.02	0.75	0.30	1.96	3.12
	–	0.97	3.48	0.84	1.06	2.80	0.76	0.31	2.02	2.95
Pseudo-triangular	+	1.26	2.55	0.86	1.28	3.40	0.59	0.35	1.70	2.49
	–	1.15	3.48	0.67	1.30	2.70	0.63	0.35	1.84	2.30

Table 4
Reference acceleration on stiff soil (type A) and soil type C.

a_{gR} (m/s^2)	Type 1.3			Type 2.3		
	DL	SD	NC	DL	SD	NC
Type A	1.17	1.50	2.60	1.33	1.70	2.95
Type C	1.35	1.73	2.99	2.00	2.55	4.43

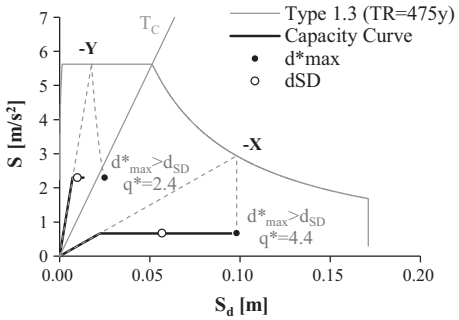

Fig. 16. Identification of the performance point in Model B for the pseudo-triangular load considering seismic action type 1.3.

aiming to limit the overall acceptable ductility. This limitation is not verified in the *X* direction due to the deformability of the building in this direction, as discussed after Table 3.

The procedure described in Fig. 16 was applied to all cases. The final results are plotted in Fig. 17 in terms of ratio between the performance point (considering both seismic actions) and the maximum displacement compatible with the fulfilment of each limit state (d^*_{max}/d_{LS}). From Fig. 17, it can first be noticed that seismic action type 1.3 is the most demanding case as the performance point is always higher than the limit displacement ($d^*_{max}/d_{LS} > 1$).

In the *X* direction, DL limit state is clearly penalized as the expected displacement is, in average, 3.5 times higher than the maximum. Nevertheless, the *Y* direction is the most vulnerable direction of the building for SD and NC limit states. With action type 2.3, the thresholds are not complied in the *Y* direction and in the *X* direction are close to it. As the verification as to be satisfied in both structural directions, it can be concluded that the building does not fulfil the performance requirements considering both seismic actions.

Finally, results are discussed in terms of ratio between the ground acceleration and the maximum acceleration compatible with the fulfilment of each limit state ($a_{gR}/a_{g,max}$), summarized in Table 5. The value of $a_{g,max}$ was determined by Eqs. (3.1) and (3.2) considering $q^* < 3$. In the following equations, *S* is the soil factor and η the damping correction factor.

$$A_{g,max} = \frac{f_y^*/m^*}{2.5s\eta}\left[1 + \frac{T^*}{T_c}\left(\frac{d_{LS}^*}{f_y^*/m^*(T^*/2\pi)^2} - 1\right)\right] \quad \text{for } T^* < T_c \qquad (3.1)$$

$$A_{g,max} = \frac{d_{LS}^*}{2.5S\eta}\frac{(2\pi)^2}{T^*T_c} \quad \text{for } T^* \geq T_c \qquad (3.2)$$

Fig. 18 plots the worst scenario between modelling solution and load distribution. As referred, the condition $q^* < 3$ is imposed by the Italian code [18] in order to limit the overall acceptable ductility of the building. As shown in Fig. 18(a), this limitation is particularly important in the *X* direction. For instance, with seismic action type 1.3 and NC limit state, q^* is equal to 6.6. Moreover, after applying this limit, the *X* direction is the most vulnerable direction of the building for seismic action type 1.3 (Fig. 18(b)). On this, it is estimated that for NC limit state the reference ground acceleration is 2.2 times higher than the maximum admissible acceleration on the structure. In the *Y* direction, the acceleration is 1.2 times higher than the limit.

After all things considered, the results from this case study confirmed the global seismic vulnerability of the building and the need of improving: (1) the in-plane capacity of the walls, in terms of ductility in the *Y* direction and in terms of overall strength in the *X* direction (most of the cases $q^* > 3$) and (2) the load transfer between walls by stiffening the timber floors. This would improve

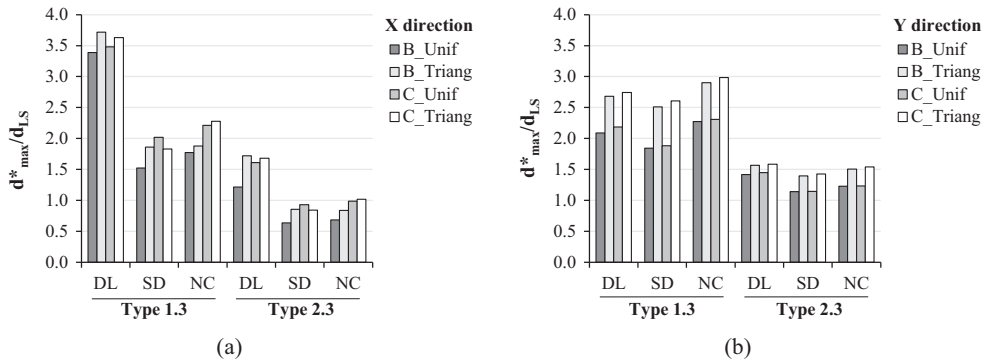

Fig. 17. Ratio between the performance point and maximum displacement compatible with the limit states: (a) *X* direction and (b) *Y* direction.

Table 5
Ratio between the reference ground acceleration and the maximum acceleration compatible with the fulfilment of each limit state: the values in bold do not verify the safety condition.

$a_{gR}/a_{g,max}$			Type 1.3			Type 2.3		
			DL	SD	NC	DL	SD	NC
B	Uniform	+X	0.88	**1.08**	**1.59**	**1.22**	0.63	0.68
		−X	**1.13**	**1.39**	**2.05**	**1.57**	0.70	0.92
	Triangular	+X	0.85	**1.04**	**1.54**	**1.72**	0.86	0.81
		−X	**1.20**	**1.47**	**2.18**	**1.72**	0.86	0.81
C	Uniform	+X	**1.16**	**1.43**	**2.11**	**1.61**	0.61	0.94
		−X	**1.13**	**1.39**	**2.06**	**1.57**	0.93	0.92
	Triangular	+X	**1.21**	**1.49**	**2.20**	**1.68**	0.84	0.98
		−X	**1.13**	**1.38**	**2.05**	**1.56**	0.81	0.91
C	Uniform	+Y	0.98	**1.04**	0.89	1.37	**1.13**	**1.22**
		−Y	**1.03**	**1.08**	0.94	**1.41**	**1.14**	0.83
	Triangular	+Y	**1.16**	**1.30**	**1.11**	**1.46**	**1.40**	0.85
		−Y	**1.25**	**1.35**	**1.21**	**1.56**	**1.39**	0.91

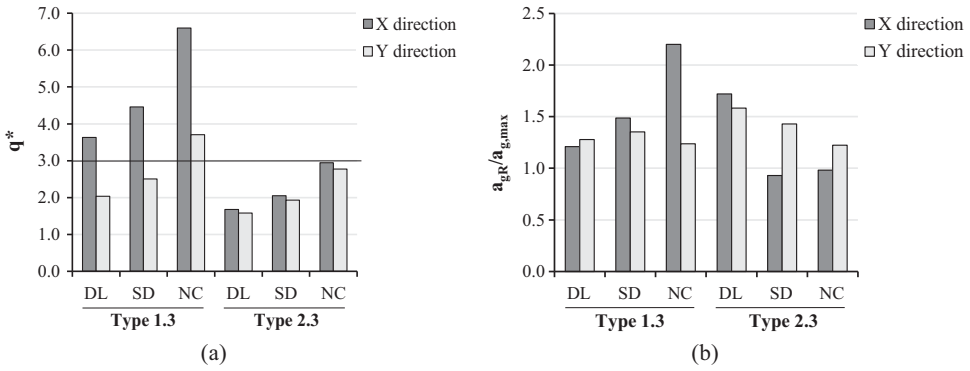

Fig. 18. Results in terms of: (a) ratio q^* and (b) ratio between reference ground acceleration and the maximum acceleration compatible with the fulfilment of each limit state.

not only the redistribution of actions among walls but also limit the concentration of damage in single walls. Finally, it is expected that the performance of the building inside the aggregate is better than that of the isolated one because of the limitation of torsional effects.

4. Local seismic behaviour

Damage observations after earthquakes have shown that unreinforced masonry buildings are prone to local failure modes related to out-of-plane mechanisms of walls [20,36,37]. This type of behaviour happens when the wall-to-wall and wall-to-floor connections are poor. These local mechanisms often occur before the attainment of the global limit states of the building (§3); however, in this paper, they are considered after because the seismic input associated with these mechanisms was defined taking into account the filtering effect of the building by means of a floor response spectra. Thus, for each limit state the seismic input was determined assuming the building has reached the same limit state at global scale (this is the most demanding condition).

In what concerns the local mechanisms, it is reasonable to consider the collapse involving only the upper level of the façade wall. Although it is evident the whole façade is very slender (17 m height with decreasing thickness), there are many constraints that give stability to the out-of-plane behaviour, such as, the connection to the side walls and the orientation of the timber floors perpendicular to the façade walls. Concerning this latter, even if there is no specific connection between timber beams and masonry walls, the friction contribution is sufficient to prevent the global overturning of the façade. The hypothesis of limiting the out-of-plane behaviour to the top floor is also supported by experimental evidence from shaking table tests of "Gaioleiro" building reduced scale models [12–14]. Thus, analysing the constructive details of the 4th floor (Fig. 19), three possible mechanisms were identified: the overturning of the central pier (Mech-1), the flexural mechanism of the central pier with a hinge separating the element in two blocks (Mech-2) and the overturning of the parapet (Mech-3). Mech-1 refers to the actual condition of the building, while Mech-2 and Mech-3 to a possible strengthened state, in which Mech-1 is prevented.

The selection of these mechanisms is supported by the following motivations. Concerning Mech-1, the two central piers with 2.0×3.3 m are more vulnerable to overturning than the lateral piers with 0.9×3.3 m as they are connected to the side walls. The lintels that link lateral and central piers are very slender elements (0.5 m height) and prone to rotate around a vertical axis with torsional sliding on the masonry joints (the friction contribution is close to zero because the vertical loads are very low at this level). From the configuration of the main façade in Fig. 19(a), central piers have a door on one side and a window on the other; the possible restraint provided by the masonry panel below the window was neglected due to its lower thickness (0.3 m). Although central piers have a perpendicular brick wall (walls P12 and P16 in Fig. 4(c)), it has been considered that the interlocking between these walls is not effective (this assumption is coherent with Model C). The roof king timber trusses are placed perpendicular to the façade walls and aligned with the central piers (Fig. 19). Assuming the king trusses are connected to the interior walls and simply supported on the façade walls, in case of the

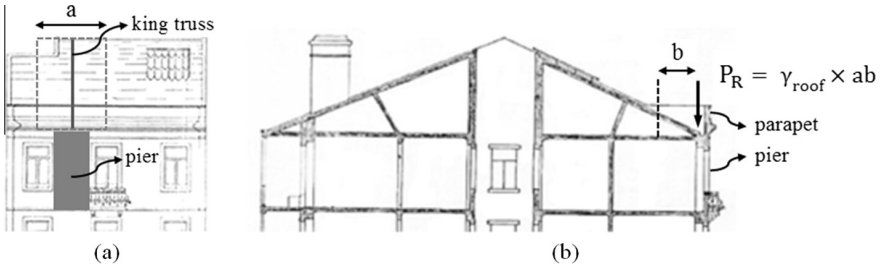

Fig. 19. View of the 4th floor: (a) façade wall and (b) section cut.

overturning of the central piers, the king trusses will slide and unthread, transmitting a stabilizing horizontal force to the piers which is equivalent to the vertical load transmitted to the piers (P_R) multiplied by a friction coefficient ($\mu = 0.2$).

As discussed more in detail in the following, Mech-1 revealed to be quite vulnerable to seismic action type 1.3. Thus, the effects of some strengthening solutions, aiming to restrain the horizontal displacement on top of the central piers, were analysed. Possible solutions are: improving the connection with the king truss, insertion of tie-rods aligned with interior walls or bracing system in the roof. After this, the most likely mechanism is the flexural mechanism of the central piers (Mech-2), which was also confirmed by the experimental results in [12] and discussed in [38]. The height of the hinge ($Z = 2.08$m) was calculated to minimize the static multiplier of the mechanism. Finally, the overturning of the parapet (Mech-3) has to be considered.

Fig. 20 shows the configuration and actions on the three local mechanisms considered: P_1 and P_2 are, respectively, the central pier and the parapet self-weight, equal to 62.7 kN and 12.2 kN; P_R, equal to 8.2 kN, is applied at 1/3 of the support length of the king truss on top of the façade; α is the coefficient proportional to the weight (P_1 and P_2) that induces the loss of equilibrium of the system (and activates the kinematism), also denominated as static horizontal load multiplier. In this case, α is equal to 0.17 for Mech-1, 1.01 in case of Mech-2 and 0.16 for Mech-3.

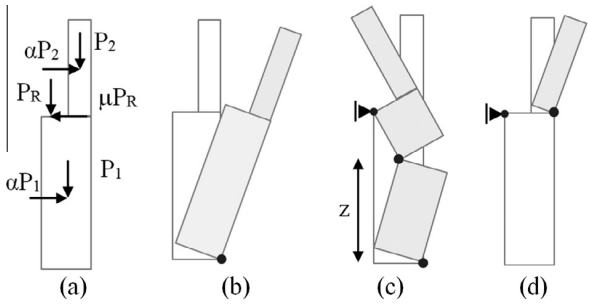

Fig. 20. Configuration and actions involved on the local mechanisms: (a) actions on the pier, (b) overturning of the simply supported central pier (Mech-1), (c) flexural mechanism of the central pier (Mech-2) and (d) overturning of the parapet (Mech-3).

The local mechanisms were analysed by the MB (Macro-Block) Perpetuate Program [5] so to perform static limit incremental analysis (following a non-linear kinematic approach). The capacity curves display the static horizontal load multiplier for increasing displacements of a control node of the kinematism. According to what was discussed in [38] and more recently in [37], the capacity curve includes the definition of an initial branch (representative of the pseudo-elastic phase) based on a bi-linear model and two distinct periods: the elastic period of the SDOF (T_e) and the secant period (T_s) from the intersection with the capacity curve. Fig. 21 plots the capacity curves of the three mechanisms in terms of spectral coordinates.

In Mech-1, the sudden decay of strength after 0.18 m displacement is consequence of the complete unthreading of the king truss. After restraining the displacement on the top of the central piers, Mech-2 can occur and, as expected, the strength increases significantly but with a reduction of the displacement capacity. Mech-3, which involves only the parapet, is the most critical mechanism as it exhibits the lowest strength and displacement capacity due to the very limited thickness of the element.

The seismic performance-based assessment follows, in parallel with the global seismic behaviour (§3), the determination of the performance point and verification of limit states associated with increasing hazard levels. The limit states were defined according to the criteria proposed in [37], supported on results from several incremental dynamic analyses: DL is assumed coincident with the rocking activation (at the intersection between the initial branch and the capacity curve), SD and NC are equal to $0.25d_0$ and $0.4d_0$, respectively, where d_0 is the displacement in which the capacity curve is zero. The corresponding limit states (LS) are plotted in Fig. 21.

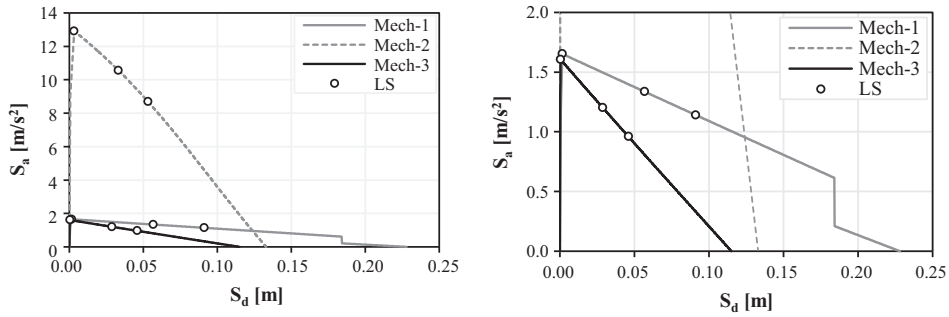

Fig. 21. Capacity curve and limit states (LS) for the analysed mechanisms (the graph on the right highlights the curves from Mech-1 and Mech-3).

Table 6
Equivalent secant period and damping of the building and local mechanisms.

Limit states	Building		Mech-1		Mech-2		Mech-3	
	$T_{k,LS}$ (s)	$\xi_{k,LS}$ (%)	$T_{k,LS}$ (s)	$\xi_{k,LS}$ (%)	$T_{k,LS}$ (s)	$\xi_{k,LS}$ (%)	$T_{k,LS}$ (s)	$\xi_{k,LS}$ (%)
DL	0.36	10.0	0.20	9.59	0.10	5.00	0.10	9.59
SD	0.41	16.3	1.30	11.92	0.35	14.31	0.97	11.92
NC	0.46	20.6	1.78	11.96	0.49	14.56	1.38	11.96

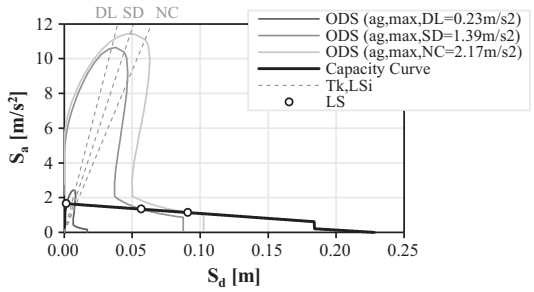

Fig. 22. Comparison between the capacity curve and the floor overdamped spectra (ODS) for Mech-1.

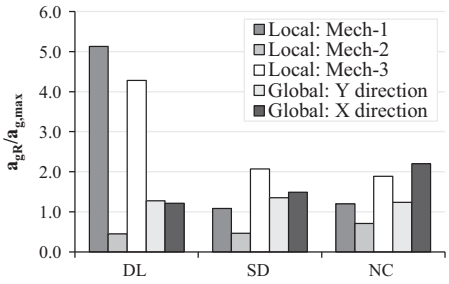

Fig. 23. Ratio between reference ground acceleration and the maximum acceleration compatible with the fulfilment of each limit state.

The performance point (d^*_{max}) was obtained from the intersection between the capacity curve and the overdamped spectrum as proposed in [37,39] and adopted in [18]. The use of the overdamped elastic response spectra is preferred to the inelastic response spectra for the following reasons: (1) the definition of the equivalent elastic period (first branch of the capacity curve), which is crucial for the N2 method [35], is affected by many uncertainties, (2) the hysteretic dissipation is very low (flag-shaped cycles) and (3) the overturning usually occurs at high values of "ductility". Since the mechanisms involve a portion of the building located at 4th floor, the seismic demand requires the definition of a response spectra that takes in account the filtering effect provided by the structure at that level. The results from the global analysis of the building (§3) were used to calibrate in more detailed way such effect. The floor response spectra were computed for each limit state based on the progressing non-linear response of the building by adopting an equivalent secant period of the structure ($T_{k,LS}$). This value was derived from the pushover analysis of the building in the *Y* direction considering Model C and the pseudo-triangular load distribution, as it provides more conservative results, and the limit states defined by the criteria discussed in §3.2. The corresponding equivalent damping ($\xi_{k,LS}$) were determined by applying some common expression proposed in the literature [40]. The activation of local mechanisms that involve portions at upper levels (as those examined) slightly affects the overall dynamic behaviour of the building (both in terms mass and stiffness). Nevertheless, results achieved on the global analysis and, herein used for the computation of the filtering effect, are considered reliable. The values adopted for each limit state are summarized in Table 6 concerning both that of the building and the local mechanisms.

Fig. 22 plots the capacity curve and the floor response spectra in case of Mech-1. The three floor overdamped spectra (ODS) correspond to the maximum acceleration ($a_{g,max}$) compatible with the fulfilment of DL, SD and NC limit states computed as in §3.2. The seismic performance-based assessment of all mechanisms is summarized in Fig. 23 based on the ratio between the ground acceleration associated with the expected hazard level and the maximum acceleration on the structure ($a_{gR}/a_{g,max}$) considering

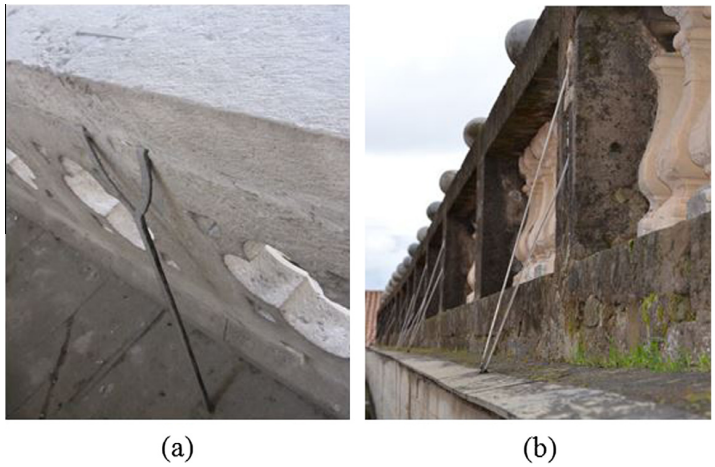

Fig. 24. Examples of (a) ancient and (b) contemporary solutions for the connection of parapets.

seismic action type 1.3. It may be observed that the "Gaioleiro" building in its actual state, in which Mech-1 and Mech-3 are possible, is very vulnerable to local mechanisms. The results show that the DL limit state is widely not verified, while the SD and NC ones present safety indexes (ratio $a_{gR}/a_{g,max}$) only slightly higher than 1, which seems consistent with the damage testified by various earthquakes. In fact, many events have highlighted that local mechanisms are quite prone to be activated by the reaching of the DL performance level, while only a limited number evolves until the complete collapse.

Therefore, some strengthening solutions aiming to solve the vulnerability associated with the out-of-plane response of the central pier (Mech-1) and the parapet (Mech-3) have to be adopted. Mech-1 may be prevented by the connection of the top of the wall with the king truss or the insertion of tie-rods aligned with interior walls. A possible intervention to mitigate the vulnerability of the parapet (Mech-3) is to fix this non-structural element at its base; Fig. 24 shows some examples of ancient and contemporary solutions. After these interventions, Mech-2 remains the only possible local mechanism, which turns out to be verified with reference to all the three limit states (Fig. 23). According to the results from Fig. 23, it is evident that the global failure of the building in the *X* direction is then the most likely to occur.

5. Conclusions

The work herein presented was addressed to the seismic performance-based assessment of an unreinforced masonry building representative of one type of "Gaioleiro" buildings. The assessment was addressed to the global seismic response of the building and to the possible activation of local mechanisms. The results highlighted that, concerning the local out-of-plane response, the building is particularly vulnerable to the overturning of the top floor central pier (Mech-1) and the parapet (Mech-3). Once adopted proper strengthening solutions to prevent such mechanisms (e.g. by improving the connection with the king truss or inserting tie-rods aligned with interior walls in case of Mech-1 and by fixing the parapet at its base in case of Mech-3), the building is not far to be verified with reference to DL and SD limit states, while it remains very vulnerable for the global NC limit state in the *X* direction. In particular, it is worth pointing out that in the direction perpendicular to the façade walls, the main criticality is related to an insufficient capacity in terms of ductility more than overall strength, while in the direction of the façade walls the opposite occurs. Thus, the improvement of the connection between perpendicular walls and between walls and horizontal diaphragms, as well as the stiffening of the latter ones, should be considered for the mitigation of seismic risk of "Gaioleiro" buildings in Lisbon.

Acknowledgements

The authors would like to acknowledge the financial support of the Portuguese Foundation for Science and Technology (Ministry of Science and Technology of the Republic of Portugal) through the research project PTDC/ECM/100872/2008 – Seismic Vulnerability of Old Masonry Buildings.

References

[1] Appleton J. Rehabilitation of "Gaioleiro" buildings. 1st edition book, Orion Editors; 2005 (in Portuguese).
[2] Lagomarsino S, Penna A, Galasco A, Cattari S. TREMURI program: an equivalent frame model for the nonlinear seismic analysis of masonry buildings. Eng Struct 2013;56:1787–99. 10.1016/j.engstruct.2013.08.002.
[3] Rota M, Penna A, Magenes G. A framework for the seismic assessment of existing masonry buildings accounting for different sources of uncertainty. Earthquake Eng Struct Dynam 2014. 10.1002/eqe.2386.
[4] Cattari S, Lagomarsino S, Bosiljkov V, D'Ayala D. Sensitivity analysis for setting up the investigation protocol and defining proper confidence factors for masonry buildings. Bull Earthquake Eng 2013. 10.1007/s10518-014-9648-3.
[5] Lagomarsino S, Ottonelli D. MB-Perpetuate – a Macro-Block program for the seismic assessment (Freeware software for the safety verification of seismic local mechanisms). PERPETUATE (EC-FP7 Project), Deliverable D29; 2012, <www.perpetuate.eu/mb/>.
[6] European Committee for Standardization (CEN). Eurocode 8: design of structures for earthquake resistance – Part 1: general rules, seismic actions and rules for buildings (EC8-1); 2004.
[7] European Committee for Standardization (CEN). Eurocode 8: design of structures for earthquake resistance – Part 3: assessment and retrofitting of buildings; 2005.
[8] Lagomarsino S, Cattari S. PERPETUATE guidelines for seismic performance-based assessment of cultural heritage masonry structures. Bull Earthquake Eng 2014. http://dx.doi.org/10.1007/s10518-014-9674-1.
[9] Lopes M, Meireles H, Cattari S, Bento R, Lagomarsino S. Pombalino constructions: description and seismic assessment, book structural Rehabilitation of Old Building. In: Aníbal Costa, João Miranda Guedes and Humberto Varum (Eds.), 2 2013 187-234, ISBN:978-3-642-39686-1.
[10] Sequeira A. Characterization and assessment of the market related to maintenance and conservation of the architectural heritage. Report GEcORPA – Grémio do Património, Lisbon, Portugal; 1999 (in Portuguese).
[11] Pinho F. Walls from Ancient Portuguese buildings. Book Collection Edifícios N° 8, Laboratório Nacional de Engenharia Civil (LNEC), Portugal; 2000, (in Portuguese).
[12] Candeias P. Assessment of the seismic vulnerability of masonry buildings. Ph.D. Thesis, University of Minho, Portugal; 2008, (in Portuguese).
[13] Mendes N, Lourenço P. Seismic assessment of masonry "Gaioleiro" buildings in Lisbon, Portugal. J Earthquake Eng 2009;14(1):80–101.
[14] Mendes N, Lourenço P, Costa A. Shaking table testing of an existing masonry building: assessment and improvement of the seismic performance. Earthquake Eng Struct Dynam 2013. 10.1002/eqe.2342.
[15] Branco M, Guerreiro L. Seismic rehabilitation of historical masonry buildings. Eng Struct 2011;33:1626–34.
[16] Silva V, Soares I. Seismic vulnerability of the "Gaioleiro" buildings of Lisbon and possible measures to reduce it. In: Proceedings of the 3rd seismology and earthquake engineering meeting, Lisbon, Portugal; 1997 (in Portuguese).
[17] Lopes M, Azevedo J. Assessment of the seismic behaviour of a Lisbon masonry building. In: Proceedings of the 3rd seismology and seismic engineering meeting, Lisbon, Portugal; 1997 (in Portuguese).
[18] Italian Code for Structural Design (Norme Tecniche per le Costruzioni – NTC). D.M. 14/1/2008, Official Bulletin N° 29 of February 4, 2008 (in Italian).
[19] Turnšek V, Sheppard P. The shear and flexural resistance of masonry walls. In: Proceedings of the international research conference on earthquake engineering, Skopje, Macedonia; 1980. p. 517–73.
[20] Magenes G, Penna A. Seismic design and assessment of masonry buildings in Europe: recent research and code development issues. In: Proceedings of the 9th Australian masonry conference, Queenstown, New Zeland; 2011 p. 583–603.
[21] 3Muri Program, S.T.A.DATA s.r.l., release 5.0.4.
[22] Lagomarsino S, Penna A, Galasco A, Cattari S. TREMURI program: seismic analyses of 3D masonry buildings, Release 2.0. Italy: University of Genoa; 2012 (mail to: tremuri@gmail.com).
[23] Calderini C, Cattari S, Degli Abbati S, Lagomarsino S, Ottonelli D, Rossi M. Modelling strategies for seismic global response of building and local mechanisms. PERPETUATE (EC-FP7 Project), Deliverable D26; 2012 <http://www.perpetuate.eu/d26>.
[24] American Society of Civil Engineers (ASCE). Seismic rehabilitation of existing buildings. USA: ASCE/SEI 41/06, American Society of Civil Engineers; 2007. ISBN:9780784408841.
[25] Cattari S, Lagomarsino S. A strength criterion for the flexural behaviour of spandrels in unreinforced masonry walls. In: Proceedings of the 14th world conference on earthquake engineering, Beijing, China; 2008.
[26] Gattesco N, Clemente I, Macorini L, Noè S. Experimental investigation of the behaviour of spandrels in ancient masonry buildings. In: Proceedings of the 14th world conference on earthquake engineering, Beijing, China; 2008.
[27] Beyer K, Mangalathu S. Review of strength models for masonry spandrels. Bull Earthquake Eng 2013;11:521–42. 10.1007/s10518-012-9394-3.
[28] Graziotti F, Magenes G, Penna A. Experimental cyclic behaviour of stone masonry spandrels. In: Proceedings of the 15th world conference on earthquake engineering, Lisbon, Portugal; 2012.
[29] Cattari S, Lagomarsino S, D'Ayala D, Novelli V, Bosiljkov V. Correlation of performance levels and damage states for types of buildings. PERPETUATE (EC-FP7 Project), Deliverable D17; 2012 <www.perpetuate.eu/d17>.
[30] American Society of Civil Engineers (ASCE). Pre-standard and commentary for the seismic rehabilitation of buildings. USA: FEMA Publication 365, Federal Emergency Management Society; 2000.
[31] Reyes J, Chopra A. Three dimensional modal pushover analysis of buildings subjected to two components of ground motion, including its evaluation for tall buildings. Earthquake Eng Struct Dynam 2011;40:789–806. 10.1002/eqe.1060.
[32] Magenes G, Della Fontana A. Simplified nonlinear seismic analysis of masonry buildings. Proc British Masonry Soc 1998;8:190–5.
[33] Abrams D. Seismic assessment and rehabilitation of unreinforced masonry buildings in the USA. In: Proceedings of the 6th national congress on seismology and earthquake engineering, Aveiro, Portugal; 2004.

[34] Mouyiannou A, Rota M, Penna A, Magenes G. Identification of suitable limit states from nonlinear dynamic analyses of masonry structures. J Earthquake Eng 2014;18(2):231–67. 10.1080/13632469.2013.842190.
[35] Fajfar P. Capacity spectrum method based on inelastic spectra. Earthquake Eng Struct Dynam 1999;28(9):979–93.
[36] D'Ayala D, Speranza E. Definition of collapse mechanisms and seismic vulnerability of masonry structures. Earthquake Spectra 2003;19(3):479–509.
[37] Lagomarsino S. Seismic assessment of rocking masonry structures. Bull Earthquake Eng 2014. 10.1007/s10518-014-9609-x.
[38] Doherty K, Griffith M, Lam N, Wilson J. Displacement-based analysis for out-of-plane bending of unreinforced masonry walls. Earthquake Eng Struct Dynam 2002;31(4):833–50. 10.1002/eqe.126.
[39] Freeman S. Development and use of capacity spectrum method. In: Proceedings of the 6th U.S. National Conference on Earthquake Engineering (NCEE), Seattle, USA; 1998. p. 269.
[40] Blandon C, Priestley M. Equivalent viscous damping equations for direct displacement based design. J Earthquake Eng 2005;9(2):257–78. 10.1142/S1363246905002390.